HHS Public Access

Author manuscript

Cell Metab. Author manuscript; available in PMC 2016 October 06.

Published in final edited form as:

Cell Metab. 2015 October 6; 22(4): 606–618. doi:10.1016/j.cmet.2015.08.018.

MSC Transplantation Improves Osteopenia *via* Epigenetic Regulation of Notch Signaling in Lupus

Shiyu Liu[1,2,3], **Dawei Liu**[1,3,4], **Chider Chen**[1,3], **Kazunori Hamamura**[3], **Alireza Moshaverinia**[3], **Ruili Yang**[1,3,4], **Yao Liu**[3], **Yan Jin**[2,*], and **Songtao Shi**[1,3,*]

[1]Department of Anatomy and Cell Biology, School of Dental Medicine, University of Pennsylvania, Philadelphia, Pennsylvania 19104, USA

[2]State Key Laboratory of Military Stomatology, Center for Tissue Engineering, School of Stomatology, The Fourth Military Medical University, Xi'an, Shaanxi 710032, China

[3]Center for Craniofacial Molecular Biology, University of Southern California, 2250 Alcazar Street, CSA 103, Los Angeles, CA 90033, USA

[4]Department of Orthodontics, Peking University School & Hospital of Stomatology, #22 Zhongguancun South Avenue, Beijing 100081, China

SUMMARY

Mesenchymal stem cell transplantation (MSCT) has been used to treat human diseases, but the detailed mechanisms underlying its success are not fully understood. Here we show that MSCT rescues bone marrow MSC (BMMSC) function and ameliorates osteopenia in Fas-deficient-MRL/*lpr* mice. Mechanistically, we show that Fas deficiency causes failure of miR-29b release, thereby elevating intracellular miR-29b levels, and downregulates DNA methyltransferase 1 (Dnmt1) expression in MRL/*lpr* BMMSCs. This results in hypomethylation of the Notch1 promoter and activation of Notch signaling, in turn leading to impaired osteogenic differentiation. Furthermore, we show that exosomes, secreted due to MSCT, transfer Fas to recipient MRL/*lpr* BMMSCs to reduce intracellular levels of miR-29b, which results in recovery of Dnmt1-mediated Notch1 promoter hypomethylation and thereby improves MRL/*lpr* BMMSC function. Collectively our findings unravel the means by which MSCT rescues MRL/*lpr* BMMSC function through reuse of donor exosome-provided Fas to regulate the miR-29b/Dnmt1/Notch epigenetic cascade.

*Corresponding Author: Songtao Shi (songtaos@dental.upenn.edu) Or Yan Jin (yanjin@fmmu.edu.cn).

AUTHOR CONTRIBUTIONS

S.L. designed and performed experiments, analyzed and interpreted data, and wrote the manuscript. D.L., C.C., K.H., A.M., R.Y., and Y.L. performed experiments and analyzed and interpreted data. Y.J. and S.S. designed experiments, analyzed data, wrote the manuscript and supervised the laboratory studies.

Competing interests: The authors declare that they have no competing interests.

SUPPLEMENTAL INFORMATION

Supplemental Information includes experimental procedures and eight figures (Figures S1-S7).

Accession numbers. The accession number for the data reported in this paper is GEO: GSE56041.

Abstract

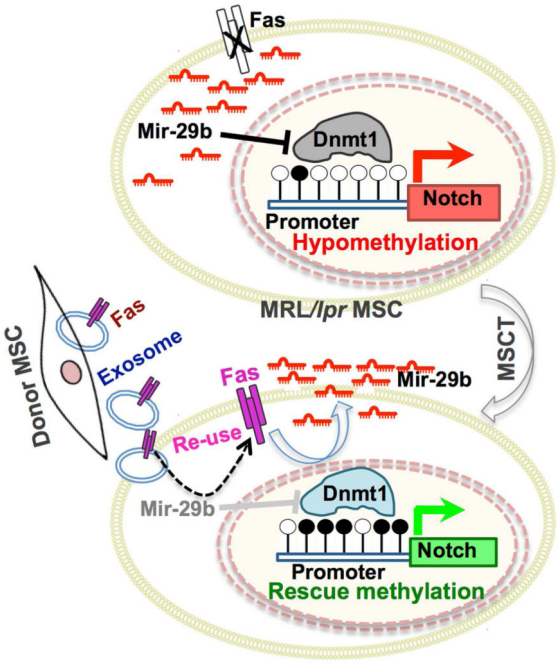

INTRODUCTION

Systemic mesenchymal stem cell transplantation (MSCT) has been successfully used to treat a variety of human diseases, such as systemic lupus erythematosus (SLE), graft versus host disease (GvHD), rheumatoid arthritis, myocardial infarction, liver fibrosis, inflammatory bowel disease, and multiple sclerosis (Augello et al., 2007; Gonzalez et al., 2009; Hatzistergos et al., 2010; Le Blanc et al., 2004; Liang et al., 2009; Ren et al., 2012; Sakaida et al., 2004; Sun et al., 2009). Multiple therapeutic mechanisms may contribute to MSCT-based therapies, including paracrine secretion of cytokines (Choi et al., 2011; Nemeth et al., 2009) and interplay between MSCs and immune cells (Akiyama et al., 2012). However, the details of these mechanisms are not fully understood. Although most systemically-infused MSCs fail to engraft into recipient organs, a single administration of MSCT is capable of perpetual amelioration of disease phenotypes (Akiyama et al., 2012; Le Blanc et al., 2008; Peng et al., 2011; Sun et al., 2009; Wang et al., 2012), suggesting that MSCT may target recipient cellular and molecular regulation to maintain MSCT-based therapeutic effects.

Epigenetic modifications encompass a wide range of heritable molecular changes and are often associated with human diseases (Kelly et al., 2010; Portela and Esteller, 2010). Epigenetic aberrations may play an important role in the maintenance of pathological status in some diseases (Bechtel et al., 2010; Golden et al., 2013; Zhang et al., 2011). Therapeutic approaches aimed at reversing epigenetic aberrations can sustain therapeutic effects (Tsai et al., 2012b). This evidence suggests that epigenetic modifications may play a crucial role in generating an epigenetic “memory” that maintains physiological and pathological status. In this study, we show that MSCT rescues impaired bone marrow MSCs (BMMSCs) and

osteoporotic phenotype in Fas-deficient MRL/*lpr* mice, which model SLE, *via* reuse of donor exosome-derived Fas to recover Fas functions.

RESULTS

MSCT rescues impaired BMMSCs and osteoporotic phenotype in recipient MRL/*lpr* SLE mice

SLE is an autoimmune disease with the potential to damage multiple organs, such as the musculoskeletal, renal, cardiovascular, neural and cutaneous systems (Rahman and Isenberg, 2008). MSCT can effectively rescue the disease phenotypes in SLE patients (Sun et al., 2009). Although the MSCs delivered during treatment usually fail to engraft to a significant degree in recipient organs, a single administration of MSCT is capable of sustained amelioration of disease phenotypes in a mouse model of SLE (MRL/*lpr* mice) (Sun et al., 2009). We revealed that BMMSCs derived from MRL/*lpr* mice showed a reduced capacity for osteogenic differentiation, as indicated by decreased calcium nodule formation and expression of osteogenic markers Runx2 and ALP when cultured under osteogenic inductive conditions (Figures 1A and S1A). We further revealed that MRL/*lpr* BMMSCs exhibited significantly reduced capacities to generate new bone when implanted into immunocompromised mice subcutaneously using hydroxyapatite tricalcium phosphate (HA/TCP) as a carrier (Figures 1B and S1B). The impaired function of MRL/*lpr* BMMSCs was rescued by MSCT at both 4 weeks and 12 weeks post-infusion, as indicated by increased mineralized nodule formation, expression of Runx2 and ALP, and *in vivo* bone formation when implanted into immunocompromised mice (Figures 1A, 1B, S1A and S1B). These results indicate that MSCT is capable of long-term rescue of the impaired function of recipient BMMSCs in MRL/*lpr* mice. When compared with wild-type control mice (C3H/HeJ), the femurs of MRL/*lpr* mice showed an osteoporotic phenotype, as indicated by significantly reduced trabecular bone volume, bone mineral density (BMD), and bone volume/total volume (BV/TV) (Figures 1C and S1C). Moreover, MRL/*lpr* mice showed reduced capacity to form new bone, as assessed by dynamic bone histomorphometric parameters, including mineral apposition rate (MAR) and bone formation rate per bone surface (BFR/BS) values using double calcein labeling (Figures S1D and S1E). At 4 weeks post-MSCT, osteoporotic phenotypes of MRL/*lpr* mice, including trabecular bone volume, BMD, and BV/TV, were rescued (Figure 1C). More importantly, MSCT-mediated rescue of osteoporotic phenotypes was retained until at least 12 weeks post-MSCT (Figure S1C). Meanwhile, the impaired capacity to form new bone seen in MRL/*lpr* mice was rescued at 4 and 12 weeks post-MSCT (Figures S1D and S1E). These data suggest that a single administration of MSCT is capable of rescuing osteoporotic phenotypes and maintaining the therapeutic effects for a sustained period of time.

Since bone homeostasis is maintained by the interplay between bone resorption by osteoclasts and bone formation by osteoblasts, we confirmed that elevated levels of RANKL and reduced levels of OPG in MRL/*lpr* mice were rescued at 4 weeks post-MSCT (Figures S1F and S1G) as well as at 12 weeks post-MSCT (Figures S1H and S1I), suggesting that MSCT improves function of both osteoblast and osteoclast lineages.

DNA methylation contributes to MSCT-mediated functional improvement of recipient MRL/*lpr* BMMSCs

Since our data showed that MSCT resulted in long-term functional improvement of MRL/*lpr* BMMSCs (Figures S1A-S1C and S1E), we next examined whether epigenetic regulation, such as DNA methylation, is involved in MSCT-mediated functional recovery of recipient MRL/*lpr* BMMSCs. DNA methylation microarray analysis showed that the global methylation pattern of MRL/*lpr* BMMSC gene promoters, as indicated by the shape of the MA-plot, was significantly different from that of control BMMSCs (Figure 1D). At one week post-MSCT, the altered global methylation pattern in MRL/*lpr* BMMSCs was partially rescued, showing a similar pattern to that observed in control BMMSCs (Figure 1D). Moreover, using unsupervised clustering analysis, we revealed that the methylation pattern of BMMSCs derived from MSCT-treated MRL/*lpr* mice was more strongly correlated with that of control BMMSCs than with that of untreated MRL/*lpr* BMMSCs (Figure S2A). In addition, whole genome methylation status analysis showed that the reduced number of methylated peaks and sum of methylated peaks in MRL/*lpr* BMMSCs were rescued by MSCT (Figures S2B and S2C), confirming that MSCT is able to rescue the global hypomethylation profile of the recipient BMMSCs.

In order to assess whether the global hypomethylation status contributes to BMMSC impairment in MRL/*lpr* mice, we used 5-Azacytidine, a demethylating agent, to induce a global hypomethylation status in wild-type BMMSCs, mimicking MRL/*lpr* BMMSCs. We found that 5-Azacitidine treatment was able to inhibit osteogenic differentiation of BMMSCs, as indicated by reduced capacity to form mineralized nodules (Figure S2D). To examine whether rescue of the global hypomethylationin MRL/*lpr* BMMSCs contributes to MSCT-mediated therapeutic effects, we used 5-Azacytidine to treat MRL/*lpr* mice at one week post-MSCT and found that 5-Azacytidine treatment blocked MSCT-mediated therapeutic effects, including the improved *in vitro* mineralized nodule formation, expression of Runx2 and ALP, *in vivo* new bone formation, trabecular bone volume, BMD and BV/TV of the femurs (Figures 1E-1G) seen after MSCT in MRL/*lpr* mice without 5-Azacytidine treatment. Also, 5-Azacytidine treatment blocked MSCT-mediated therapeutic improvement of the capacity for new bone formation in MRL/*lpr* mice, as assessed by MAR and BFR/BS values (Figure S2E). These results indicate that global DNA methylation status may be essential for MSCT-mediated rescue of recipient BMMSC function and osteoporotic phenotype in MRL/*lpr* mice.

Notch1 promoter methylation contributes to MSCT-mediated functional improvement of recipient MRL/*lpr* BMMSCs

Given that MSCT rescues the hypomethylation status in recipient BMMSCs, we next evaluated whether DNA hypomethylation occurred in any specific gene in recipient BMMSCs that may contribute to MSCT-mediated therapeutic rescue. Based on DNA methylation array analysis, we found that, compared with wild-type BMMSCs, several of the Notch genes, including Notch1, Notch2, Jag1, Jag2, DLL4, and Hes5, were hypomethylated in MRL/*lpr* BMMSCs and this hypomethylation status was rescued by MSCT (Figures S2F-S2K). Since Notch signaling has been demonstrated to regulate bone mesenchymal cell self-renewal and differentiation (Dong et al., 2010; Hilton et al., 2008),

we used bisulfite genomic sequencing analysis to show that the promoter region of Notch1 (−1053/−834) was hypomethylated and its methylation status was rescued after MSCT (Figures 2A, S2L and S2M). Moreover, we revealed that MRL/*lpr* BMMSCs had elevated expression levels of Notch1, Notch2, Jag1 and Notch1 intracellular domain (NICD) compared to wild-type BMMSCs; however, this elevation of Notch-related gene expression was reduced by MSCT (Figure 2B). These data indicate that hypomethylation led to the activation of Notch signaling, which was rescued by MSCT (Figure 2B).

We thus hypothesized that hypomethylation of the promoters of Notch1 activated Notch signaling, resulting in reduced osteogenic differentiation in MRL/*lpr* BMMSCs. To test this hypothesis, we treated MRL/*lpr* BMMSCs with DAPT, a Notch signaling inhibitor (Figures S3A and S3B). DAPT treatment partially rescued osteogenic differentiation capacity, as indicated by mineralized nodule formation, expression of osteogenic markers Runx2 and ALP (Figure 2C), and *in vivo* bone formation (Figure 2D). To further confirm the role of Notch signaling in the regulation of BMMSC functions, we treated MRL/*lpr* mice with DAPT and found that DAPT treatment rescued MRL/*lpr* BMMSC function, as indicated by improved *in vitro* mineralized nodule formation, expression of Runx2 and ALP (Figure 2E) and *in vivo* bone formation (Figure 2F). Moreover, *in vivo* DAPT treatment partially rescued the osteoporotic phenotype and new bone formation capacity of MRL/*lpr* mice, as indicated by increased trabecular bone volume, BMD, BV/TV, MAR and BFR/BS (Figures 2G and S3C). Moreover, DAPT treatment reversed inhibitive effects of 5-Azacytidine on MSCT-mediated therapeutic effects, as indicated by improved trabecular bone volume, BMD, BV/TV, mineralized nodule formation and expression of Runx2 and ALP (Figures S3D and S3E). In order to further confirm the role of Notch1 in regulating bone mass, we used siRNA injection to knock down Notch1 expression and found that *in vivo* knockdown of Notch1 (Figure S3F) partially rescued the osteoporotic phenotype in MRL/*lpr* mice, as indicated by elevated trabecular bone volume, BMD and BV/TV values (Figure S3G). Moreover, *in vitro* Notch1 knockdown partially rescued impaired BMMSC function in MRL/*lpr* mice, as indicated by increased mineralized nodule formation and expression of Runx2 and ALP (Figure S3H). These data indicate that DNA methylation modifications of Notch signaling play an important role in the impairment of MRL/*lpr* BMMSCs and that the function of these BMMSCs can be rescued by MSCT.

Hypomethylation of Notch1 is regulated by miR-29b-mediated downregulation of Dnmt1

We next aimed to gain insights into how the hypomethylation of the Notch 1 promoters was regulated by MSCT. DNA methylation of CpG dinucleotides is catalyzed by at least three different DNA methyltransferases (DNMTs), including Dnmt1 for methylation maintenance and Dnmt3a and Dnmt3b for *de novo* methylation (Denis et al., 2011). The DNMTs are essential for maintaining the methylation pattern in stem cells and for regulating their self-renewal and differentiation (Challen et al., 2012; Tsai et al., 2012a). We observed downregulation of Dnmt1, Dnmt3a and Dnmt3b in MRL/*lpr* BMMSCs when compared to control BMMSCs, as indicated by Western blot (Figure 3A). MSCT rescued the downregulated Dnmt1, Dnmt3a and Dnmt3b in MRL/*lpr* BMMSCs (Figure 3A). Therefore, we aimed to evaluate whether elevated expression of DNMTs as a result of MSCT contributes to the rescue of hypomethylation of the Notch1 promoter in MRL/*lpr* BMMSCs.

Using an siRNA knockdown approach, we demonstrated that Dnmt1-siRNA, but not Dnmt3a-siRNA or Dnmt3b-siRNA, inhibited BMMSC osteogenic differentiation and expression of Runx2 and ALP (Figure 3B, 3C and S4A-S4C). Thus, we focused on examining the functional role of Dnmt1 in MSCT-treated MRL/*lpr* mice. To evaluate whether Dnmt1 regulates BMMSC function through DNA methylation of Notch genes, we demonstrated that knockdown of Dnmt1 by siRNA induced hypomethylation of the Notch1 promoter (Figure 3D) and activated Notch signaling, including upregulation of Notch1, Notch2 and NICD (Figure 3E), mimicking the altered methylation and expression of the *Notch1* gene in MRL/*lpr* BMMSCs. Moreover, inhibition of Notch signaling by DAPT treatment partially rescued the Dnmt1 knockdown-induced impairment of BMMSCs, as indicated by *in vitro* osteogenic differentiation with mineralized nodule formation and expression of Runx2 and ALP (Figure 3F). Additionally, we showed that inhibition of methylation by 5-Azacytidine treatment downregulated Dnmt1 and upregulated Notch1 and NICD expression in BMMSCs (Figure S4D). These data demonstrate that Dnmt1-mediated Notch1 promoter DNA methylation contributes to MSCT-induced functional recovery of recipient MRL/*lpr* BMMSCs. Next, we showed that upregulation of Dnmt1 in MRL/*lpr* BMMSCs rescued several defects: hypomethylation of the Notch-1promoter, upregulated expression of Notch1, Notch2, and NICD, impaired *in vitro* osteogenic differentiation and reduced expression of Runx2 and ALP (Figures 3G-3I and S4E).

Given that Dnmt1 regulates the Notch1 promoter methylation and contributes to functional recovery of recipient MRL/*lpr* BMMSCs, we next determined how Dnmt1 expression is regulated in MRL/*lpr* BMMSCs, and in particular whether microRNAs are involved in this process. MicroRNAs are noncoding 22-nucleotide RNAs which serve as repressors of gene expression at the post-transcriptional regulation level and are involved in some disease processes (Soifer et al., 2007). In order to evaluate whether microRNAs are involved in the regulation of Dnmt1 expression, we used microRNA microarray analysis to show that miR-29b, which was previously demonstrated to indirectly inhibit Dnmt1 expression and induce global hypomethylation modifications (Garzon et al., 2009; Qin et al., 2013), was upregulated in MRL/*lpr* BMMSCs and downregulated after MSCT (Figures 4A and S4F). Based on these data, we hypothesized that miR-29b might govern Dnmt1-mediated DNA methylation modifications of the *Notch1* promoter, leading to the functional recovery of recipient MRL/*lpr* BMMSCs after MSCT. In accordance with previous studies (Garzon et al., 2009; Qin et al., 2013), we found that *in vitro* miR-29b inhibitor treatment reduced expression of miR-29b and increased Dnmt1 expression in BMMSCs, as indicated by real-time PCR and Western blot (Figures S4G-S4I). MiR-29b inhibitor treatment also promoted *in vitro* osteogenic differentiation of BMMSCs, as indicated by mineralized nodule formation (Figure S4J). In order to evaluate the functional role of miR-29b *in vivo*, we treated MRL/*lpr* mice with miR-29b inhibitor and found that the treatment reduced the levels of miR-29b and Notch1 while elevating expression levels of Dnmt1 in MRL/*lpr* BMMSCs (Figures 4B and 4C). Inhibitor treatment also increased mineralized nodule formation, assessed by alizarin red staining, and increased expression of Runx2 and ALP, assessed by Western blot analysis (Figure 4D). When implanted into immunocompromised mice, BMMSCs derived from miR-29b inhibitor-treated MRL/*lpr* mice showed increased capacity for *in vivo* new bone formation (Figure 4E). In addition, *in vivo* miR-29b inhibitor

treatment rescued the osteoporotic phenotype and new bone formation capacity of MRL/*lpr* mice, as indicated by increased trabecular bone volume, BMD, BV/TV, MAR and BFR/BS (Figures 4F and S4K). Meanwhile, introduction of synthesized double-stranded miR-29b into naïve BMMSCs mimics the effect of physiological modulators that increase miR-29b expression in BMMSCs (Figures S4L). MiR-29b mimics decreased the expression levels of Dnmt1 in BMMSCs, as indicated by real-time PCR and Western blot (Figures S4M and S4N). MiR-29b mimics also reduced *in vitro* osteogenic differentiation of BMMSCs, as indicated by mineralized nodule formation (Figure S4O). In order to explore whether miR-29b-mediated DNA methylation modifications are associated with regulation of Notch signaling, we demonstrated that miR-29b mimics resulted in hypomethylation of the *Notch1* promoter (Figure 4G), leading to high levels of Notch1, Notch2, Jag1 and NICD expression compared to the control group (Figure 4H). In accordance with the results regarding Notch signaling function, the miR-29b mimics inhibited *in vitro* osteogenic differentiation of BMMSCs, as indicated by mineralized nodule formation and expression of Runx2 and ALP (Figure 4I). These effects were partially attenuated by treatment with the Notch inhibitor, DAPT (Figure 4I). These data suggest that MSCT regulates miR-29b/Dnmt1/Notch signaling to achieve long-term functional recovery of MRL/*lpr* BMMSCs.

Exosomes secreted due to MSCT rescue MRL/*lpr* BMMSC function

Next, we examined how MSCT regulated the levels of miR-29b in recipient MRL/*lpr* BMMSCs. When MRL/*lpr* BMMSCs were co-cultured with wild-type BMMSCs in a transwell system, elevated intracellular levels of miR-29b, altered expression of Dnmt1, Notch1, and NICD, and reduced *in vitro* osteogenic differentiation in MRL/*lpr* BMMSCs were rescued, as assessed by real-time PCR, Western blot, and alizarin red staining, respectively (Figures 5A, 5B and S5A). These data suggest that wild-type BMMSCs may release soluble factors or vesicles to regulate MRL/*lpr* BMMSCs, perhaps by secreting exosomes. Exosomes are small membrane vesicles (30-100 nm) of endocytic origin that are constitutively released *via* fusion with the cell membrane (Thery et al., 2002). Exosomes can mediate local and systemic cell-cell communications through the transfer of proteins, mRNAs and microRNAs (Mittelbrunn and Sanchez-Madrid, 2012). In order to test whether BMMSCs secrete exosomes to rescue MRL/*lpr* BMMSC function, we used a siRNA approach to knockdown the expression of rab27a, a promoter for exosome secretion, to block exosome secretion (Figures S5B and S5C) (Ostrowski et al., 2010). We found that siRNA knockdown of rab27a attenuated BMMSC-mediated rescue of intracellular levels of miR-29b and expression of Dnmt1, Notch1 and NICD, as well as *in vitro* osteogenic differentiation in MRL/*lpr* BMMSCs (Figures 5A, 5B and S5A). In order to further evaluate the role of exosomes in MSCT-mediated *in vivo* rescue of recipient MRL/*lpr* BMMSCs, we revealed that knockdown of rab27a by siRNA blocked MSCT-induced reduction of intracellular levels of miR-29b, upregulation of Dnmt1 and downregulation of Notch1 and NICD, while elevating mineralized nodule formation and upregulating Runx2 and ALP in MRL/*lpr* BMMSCs (Figures 5C-5F).

Next, we evaluated the direct effects of exosomes on MRL/*lpr* BMMSCs. We first confirmed that BMMSC-derived exosomes express CD63 and CD81 using Western blot (Figure S5D). When intravenously infused into MRL/*lpr* mice, exosomes were detected in

bone marrow cells at 24 hours post-infusion (Figure S5E). When added to cultured MRL/*lpr* BMMSCs, exosomes were taken in by BMMSCs (Figure S5F) and the levels of intracellular miR-29b were reduced (Figure S5G), while Dnmt1 was upregulated (Figure S5H), *in vitro* osteogenic differentiation was improved (Figure S5I) and *in vivo* bone formation was increased (Figure S5J). These data indicate that exosomes play an essential role in the regulation of miR-29b levels and rescue of MRL/*lpr* BMMSC functions.

To verify whether exosomes exert therapeutic effects *in vivo*, we infused exosomes into MRL/*lpr* mice and found that exosome infusion significantly reduced the intracellular levels of miR-29b (Figure 5G), upregulated expression of Dnmt1 and downregulated expression of Notch1 and NICD (Figure 5H), elevated mineralized nodule formation and expression of Runx2 and ALP (Figure 5I) and increased *in vivo* bone formation (Figure 5J) in MRL/*lpr* BMMSCs. Exosome infusion produced similar effects to those observed in MSCT groups. Moreover, exosome infusion increased trabecular bone volume, BMD, BV/TV, MAR and BFR/BS in MRL/*lpr* mice (Figures 5K and S5K).

MRL/*lpr* BMMSCs reuse Fas, provided by donor exosomes, to rescue their functions

We next aimed to gain insights into how exosomes regulate the intracellular levels of miR-29b in recipient MRL/*lpr* BMMSCs. Although MRL/*lpr* BMMSCs had elevated levels of intracellular miR-29b, they showed reduced levels of miR-29b in culture medium, serum and bone marrow (Figures S6A-S6C). These reduced levels of miR-29b were rescued by MSCT (Figures S6A-S6C). We further revealed that MRL/*lpr* BMMSCs showed reduced levels of the initial transcription product pri-miR-29b (Figure S6D), suggesting that production of miR-29b is not significantly increased, but failure of MRL/*lpr* BMMSCs to release miR-29b into the extracellular compartment may result in increased intracellular levels and reduced extracellular levels of miR-29b. Since MRL/*lpr* mice have a significant Fas deficiency and it is known that Fas controls the MCP-1 secretion in BMMSCs (Akiyama et al., 2012), we sought to determine whether Fas controls miR-29b secretion in BMMSCs. We found that siRNA knockdown of Fas in wild-type BMMSCs increased the levels of intracellular miR-29b and decreased the levels of extracellular miR-29b (Figures 6A, 6B and S6E), the same as observed in MRL/*lpr* BMMSCs. However siRNA knockdown of Fas in BMMSCs failed to significantly affect expression of pri-miR-29b (Figure S6F). Meanwhile, overexpression of Fas in MRL/*lpr* BMMSCs decreased the levels of intracellular miR-29b and increased the levels of extracellular miR-29b (Figures 6C, 6D and S6G), as was observed in MSCT-treated MRL/*lpr* BMMSCs. Additionally, overexpression of Fas failed to significantly affect the levels of pri-miR-29b (Figure S6H). These data suggest that Fas may control miR-29b secretion in BMMSCs.

We next determined whether exosomes regulated the levels of miR-29b through rescue of Fas-mediated miR-29b release in MRL/*lpr* BMMSCs. We found that exosomes indeed contained Fas protein (Figure S6I). More interestingly, in a co-culture system, exosomes from wild-type BMMSCs decreased intracellular levels of miR-29b and increased extracellular levels of miR-29b in MRL/*lpr* BMMSCs (Figures 6E and 6F). However, exosomes derived from MRL/*lpr* BMMSCs failed to reduce intracellular miR-29b levels (Figures 6E and 6F). Exosomes derived from MRL/*lpr* BMMSCs failed to rescue the

osteoporotic phenotype in MRL/*lpr* mice, as assessed by trabecular bone volume, BMD and BV/TV, when compared to exosomes derived from wild-type BMMSCs (Figure 6G). Moreover, exosomes derived from MRL/*lpr* BMMSCs failed to rescue impaired osteogenic differentiation of recipient MRL/*lpr* BMMSCs, as assessed by mineralized nodule formation and the expression of Runx2 and ALP (Figure 6H). These data indicate that Fas plays an essential role in exosome-mediated recovery of miR-29b secretion.

We therefore hypothesized that exosomes may be able to transfer functional Fas to MRL/*lpr* BMMSCs to restore Fas-mediated miR-29b release. To test this hypothesis, we transfected BMMSCs with plasmids expressing Fas-enhanced green fluorescent protein (Fas-eGFP) and used them to generate Fas-eGFP exosomes (Figure S6J). We used immunofluorescent staining and flow cytometric analysis to show that Fas-eGFP fusion protein could be transferred to MRL/*lpr* BMMSCs after treatment with Fas-eGFP-exosomes both *in vitro* and *in vivo* (Figures 7A-C). Interestingly, when lysosome inhibitor was used to block lysosome functions, Fas-eGFP fusion protein failed to locate on the BMMSC membrane (Figure 7D). Therefore, Fas reuse in MSCT appears to occur through non-direct membrane fusion. In a transwell co-culture system, activated T cells were capable of inducing BMMSCs to undergo apoptosis *via* the FasL/Fas pathway (Figures 7E and 7F). Due to the lack of functional Fas in MRL/*lpr* BMMSCs, activated T cells failed to induce them to undergo apoptosis (Figure 7G). However, treatment with exosomes derived from either wild-type BMMSCs or Fas-overexpressed MRL/*lpr* BMMSCs, but not from MRL/*lpr* BMMSCs, restored the ability of activated T cells to induce MRL/*lpr* BMMSC apoptosis (Figure 7G). This apoptosis process was blocked by FasL neutralized antibody (Figure 7G). These results suggest that exosomes can transfer functional Fas to MRL/*lpr* BMMSCs, leading to rescue of intracellular miR-29b release and Fasl/Fas-mediated apoptosis. In order to evaluate whether MSCT generated other therapeutic effects, we infused either MSCs or exosomes into MRL/*lpr* mice and examined their effect on reducing lymph node mass. We found that MSCT or exosome infusion was able to reduce the size of the lymph nodes and spleen at 4 and 8 weeks post transplantation, respectively (Figure S7A-F). In addition, infusion of CD63-EGFP-labeled BMMSCs or exosomes transferred Fas to T cells and restored T cell apoptosis in MRL/*lpr* lymph nodes (Figure S7G-J).

DISCUSSION

Since the first cell-based therapy using hematopoietic stem cell (HSC) transplantation was successfully performed in 1959 (Copelan, 2006), HSCs, MSCs and neural stem cells (NSCs) have been used to treat various human diseases (Uccelli et al., 2008). Although multiple mechanisms, such as secretion of cytokines/chemokines and cell-cell interactions, have been proposed to be responsible for MSC-based immune therapies, it has remained unclear whether cell-based therapies use epigenetic regulation to achieve therapeutic effects. In this study, we found that systemic MSCT rescued impaired recipient MRL/*lpr* BMMSCs *via* regulation of DNA methylation status. This may explain why administering MSCT once can provide long-time therapeutic effects (Akiyama et al., 2012; Le Blanc et al., 2008; Sun et al., 2009). Although we focused on epigenetic modifications to the recipient MRL/*lpr* BMMSCs, we could not exclude the possibility that the MSCT triggered epigenetic modifications in other types of cells in the recipient as well. Previous studies showed that

the T cells in human SLE patients and SLE mice are also hypomethylated and exhibit downregulated expression of DNMTs (Pan et al., 2010; Qin et al., 2013) while their levels of Notch signaling are elevated (Teachey et al., 2008). Additional experiments are required to examine whether MSCT offers therapeutic benefits to immune cells in MRL/*lpr* mice.

A significant advantage of cell-based therapy is that the infused cells exert therapeutic effects in multiple ways that are responsive to different host microenvironments (Bernardo and Fibbe, 2013; Li et al., 2012). These properties may account for why MSCT has shown therapeutic effects in a variety of disease conditions. In this study, we found MSCT rescued the global hypomethylation pattern of the recipient BMMSCs, thereby using epigenetic regulation to achieve a therapeutic effect. These findings indicate that other types of cell-based therapies may also use epigenetic regulation as one of their therapeutic mechanisms. MircoRNAs play a critical role in stem cell differentiation and self-renewal. Emerging evidence indicates that multiple miRNAs are capable of regulating the osteogenic differentiation of MSCs and maintaining bone homeostasis (Clark et al., 2014; Li et al., 2015). In this study, we reveal that recipient MSCs are capable of receiving exosomes from donor MSCs and reusing Fas derived from the exosomes to improve mir-29b release, resulting in a recovery of a mir-29b-mediated epigenetic cascade to improve recipient MSC function. Since we find Fas may control the release of multiple miRNAs in MSCs, and because exosomes contain a variety of miRNAs, it is possible that MSCT-mediated exosome transfer may affect the function of multiple miRNAs and miRNA-mediated epigenetic regulation.

Aberrations in exosome-mediated cell-cell communications are believed to play an important role in the disease development process (Luga et al., 2012; Peinado et al., 2012). Recent studies indicate that tumor-derived exosomes are important tumorigenesis mediators capable of educating stromal/stem cells for neoplastic transformation and tumor metastasis Peinado et al., 2012;). Meanwhile, stromal cell-derived exosomes are able to promote cancer cell migration (Luga et al., 2012). This evidence suggests that exosomes play a crucial role in biological crosstalk between tumor cells and surrounding stromal cells. Since exosomes serve as systemic cell-cell communication mediators, we could not exclude their “off-target” effects on other organs. Here we found MSCT or exosome infusion successfully reduced lymph node mass in MRL/*lpr* mice through Fas reuse-mediated T cell apoptosis. These results indicate that MSC-derived exosomes generate “off-target” effects and MSCT may use multiple mechanisms to achieve therapeutic effects. MSCT-mediated detailed therapeutic effects need to be further explored in the future study. Given the crucial roles of miRNAs in regulating gene expression and in disease development, miRNAs are regarded as potential therapeutic targets using chemically modified miRNA-targeting antisense oligonucleotides (Li and Rana, 2014). Previous studies showed that miR-29 regulates osteoblastic differentiation (Kapinas et al., 2010; Li et al., 2009). Here, we found that miR-29b inhibitor treatment rescued the osteoporotic phenotype and BMMSC-mediated new bone formation in MRL/*lpr* mice. This evidence indicates that multiple miRNAs other than miR-29b could be potential therapeutic targets for intervention. Previous study demonstrated that MSCT could transfer mitochondria to the recipient pulmonary alveoli (Islam et al., 2012), suggesting that MSCT may provide organelles to the recipient organs that assist in

the rescue of the host cells. Although we reveal that the cellular component Fas can be transferred to the recipient MSCs in MRL/lpr mice and rescue their impaired stem cell functions, it is unknown how Fas is transferred and how long it can be retained in the recipient cells. Also, it will be very interesting to understand whether MSCT-derived exosomes can transfer cellular components other than Fas to the recipient cells. Therefore, it is necessary to further explore detailed molecular and cellular mechanisms in MSCT therapies, especially in MSCT-mediated exosome transfer. Although it is unknown how Fas is reused in recipient MRL/*lpr* BMMSCs after MSCT, it is possible that intracellular metabolism, such as proteasome-mediated degradation, contributes to the process of Fas reuse.

EXPERIMENTAL PROCEDURES

Mice

Female C3MRL-Fas^{lpr}/J (MRL/*lpr*) and C3H/HeJ mice were purchased from the Jackson Laboratory (Bar Harbor, Maine, USA). Female immunocompromised mice (Beige XIDIII nude/nude) were purchased from Harlan (Denver, CO, USA). All animal experiments were performed under institutionally approved protocols for the use of animal research (University of Pennsylvania IACUC# 805478 and University of Southern California IACUC #11953).

Isolation of mouse bone marrow mesenchymal stem cells (BMMSCs)

A single suspension of bone marrow-derived all nucleated cells (ANCs) from mouse femurs and tibias was seeded at a density of 2.5×10^5 cells per square centimeter on 10 cm culture dish (Corning, NY, USA) at 37°C in 5% CO_2. Non-adherent cells were removed after 48 hours and attached cells were maintained for 16 days in alpha minimum essential medium (α-MEM, Invitrogen) supplemented with 20% fetal bovine serum (FBS, Equitech-Bio, Kerrville, TX, USA), 2 mM L-glutamine, 55 μM 2-mercaptoethanol, 100 U/ml penicillin and 100 μg/ml streptomycin (Invitrogen). Colonies forming attached cells were passed once for further experimental use.

BMMSC–mediated bone formation *in vivo*

Approximately 4.0×10^6 BMMSCs were mixed with hydroxyapatite/tricalcium phosphate (HA/TCP) ceramic particles (40 mg, Zimmer, Warsaw, IN, USA) as a carrier and subcutaneously implanted into the dorsal surface of 8– to 10–week–old immunocompromised mice. At 8 weeks post–implantation, the implants were harvested and were fixed with 4% paraformaldehyde (PFA) in phosphate buffered saline (PBS), decalcified with 5% EDTA in PBS, then embedded in paraffin. The 6-μm-thick sections were stained with hematoxylin and eosin (H&E). Images of the implants were analyzed using Image J software (NIH). Five fields were selected and the newly formed mineralized tissue area in each field was calculated as a percentage of the total tissue area.

Osteogenic differentiation assay

BMMSCs were cultured in osteogenic medium containing 2 mM β-glycerophosphate (Sigma), 100 μM L-ascorbicacid 2-phosphate (Sigma) and 10 nM dexamethasone (Sigma).

Ten days after osteogenic induction, total protein was extracted from cultured BMMSCs and the expression of Runx2 and ALP was assayed by Western blot analysis. After four weeks osteogenic induction, the cultures were stained with 1% alizarin red-S (Sigma). Alizarin red-positive area was analyzed using Image-J software (NIH) and shown as a percentage of alizarin red-positive area over total area.

Mesenchymal stem cell therapy (MSCT)

C3H/HeJ-derived BMMSCs at passage one were suspended in PBS (200 μl) and infused into MRL/*lpr* mice (0.1×10^6 cells per 10 g body weight) intravenously *via* the tail vein at 10 weeks of age. The MRL/*lpr* mice infused with PBS were used as MSCT controls. Background-matched C3H/HeJ mice infused with PBS were used as positive controls. Mice were sacrificed 7 days, 4 weeks or 12 weeks after MSCT for further analysis.

N-[N-(3,5-Difluorophenacetyl)-L-alanyl]-S-phenylglycine t-butyl ester (DAPT) treatments *in vitro* and *in vivo*

BMMSCs used for *in vitro* osteogenic differentiation were pretreated with DAPT (1 μM, Sigma) or DMSO (mock) for 7 days. For BMMSC–mediated bone formation *in vivo*, BMMSCs were pretreated with DAPT for 7 days and subcutaneously implanted into immunocompromised mice as described above. For *in vivo* study, mice were treated with 100 μl vehicle control (10% ethanol, 90% corn oil) or DAPT (10 mg/kg of body weight, dissolved in 10% ethanol, 90% corn oil) subcutaneously. A regimen of daily treatment was continued for 3 days followed by 4 days without treatment. This weeklong paradigm was repeated 4 times. Four weeks after the first treatment, mice were sacrificed for further analysis.

5-Azacytidine treatments *in vitro* and *in vivo*

BMMSCs used for *in vitro* osteogenic differentiation were treated with 5-Azacytidine (500 nM, Sigma) or PBS (mock) for 3 days. For *in vivo* study, 7 days after MSCT, the mice were treated with 5-Azacytidine (0.5 mg/kg of body weight, dissolved in PBS) or PBS (mock) subcutaneously for 7 days. Four weeks after MSCT, mice were sacrificed for further analysis.

Isolation, characterization and labeling of exosomes

Cells were cultured in exosome-depleted medium (complete medium depleted of FBS-derived exosomes by overnight centrifugation at 100,000g) for 48 h. Exosomes from culture supernatants were isolated by differential centrifugation, as described in the literature (Thery et al., 2006), at 300g for 10 min, 2,000g for 10 min, 10,000g for 30 min and 100,000g for 70 min, followed by washing with PBS and purification by centrifugation at 100,000g for 70 min. In each exosome preparation, the concentration of total proteins was quantified using the Pierce BCA Protein Assay (Thermo). Purified exosomes were characterized by Western blot using anti-CD63 and CD81 antibodies. PKH-26 (Sigma) was used for exosome labeling according to the manufacturer’s instructions.

Treatment with exosomes

For *in vitro* treatment, BMMSCs were pretreated with exosomes (20 μg/ml) or PBS (mock) for 3 days and then under osteoinductive culture conditions for 4 weeks. For BMMSC–mediated *in vivo* bone formation, BMMSCs were pretreated with exosomes (20 μg/ml) for 3 days and subcutaneously implanted into immunocompromised mice as described above. For *in vivo* treatments, exosomes (100 μg) suspended in 200 μl PBS or PBS (mock) was infused into MRL/*lpr* mice intravenously by the tail vein. 4 weeks after the treatment, mice were sacrificed for further analysis. For *in vivo* exosome tracking, PKH-26-labeled exosomes (100 μg) was infused into MRL/*lpr* mice intravenously by the tail vein. At 24 hours post-infusion, the femurs were fixed in 4% PFA and then decalcified with 5% ethylenediaminetetraacetic acid (EDTA), followed by optimal cutting temperature compound (OCT, Sakura Finetek, Torrance, CA, USA) embedding. Frozen sections were prepared and slides were mounted with Vectashield mounting medium containing 4′,6-diamidino-2-phenylindole (DAPI) (Vector Laboratories, Burlingame, CA, USA).

DNA methylation and microRNA microarray

Seven days after MSCT, BMMSCs derived from C3H/HeJ mice, MRL/*lpr* mice and MRL/*lpr* mice treated with MSCT were isolated and cultured as described above. For DNA methylation microarray analysis, total DNA from cells at passage one was extracted using a DNeasy Blood & Tissue Kit (Qiagen, Valencia, CA, USA) according to the manufacturer's instructions. DNA methylation microarray (MeDIP-chip) and data processing were performed using Arraystar (Rockville, MD, USA). For microRNA microarray analysis, total RNA from cells at passage one was extracted using a miRNeasy Mini Kit (Qiagen) according to the manufacturer's instructions. MicroRNA microarray and data processing were performed by LC Sciences (Houston, TX, USA).

Immunofluorescent staining

The BMMSCs were cultured on 4-well chamber slides (Nunc, Rochester, NY, USA) (2×10^3/well) and treated with exosomes (20 μg/ml) derived form BMMSCs transfected with plasmids containing Fas-EGFP fusion protein as described above. The cells were then fixed with 4% paraformaldehyde. The chamber slides were incubated with anti-GFP antibody (1:400) and anti-CD73 antibody (1:200) at 4°C overnight followed by treatment with AlexaFluoro 488-conjugated secondary antibody (1:400) and anti-rat IgG-PE secondary antibody (1:400) for 1 hour at room temperature. ActinGreen 488 Ready Probes Reagent (Life Technologies) was used for cytoskeleton staining. Finally, slides were mounted with Vectashield mounting medium containing DAPI. To evaluate the role of lysosomes in protein reuse, MRL/*lpr* BMMSCs were pretreated with lysosome inhibitor (Chloroquine, 200 μM, Sigma) for 6 hours before the treatment with Fas-EGFP$^+$ exosomes. For detection of Fas-EGFP fusion protein *in vivo*, Fas-EGFP$^+$ exosomes (100 μg) were infused into MRL/*lpr* mice intravenously by the tail vein. After 24 hours of infusion, the single suspension of bone marrow-derived cells from femurs and tibias was cultured. Five days after the culture, the colonies were used for immunofluorescent staining using antibodies against GFP and CD73. After 24 hours of Fas-EGFP$^+$ BMMSCs or Fas-EGFP$^+$ exosome

infusion into MRL/*lpr* mice, the single suspension of cells in lymph nodes was used for immunofluorescent staining using antibodies against GFP and CD3.

Statistics

SPSS 13.0 was used to perform statistical analysis. Group allocation, outcome assessment or animal studies were not done in a blinded manner. We selected sample size based on our previous studies.(Akiyama et al., 2012; Liu et al., 2011) The samples were excluded if any abnormality in terms of size, weight or apparent disease symptoms were observed in mice before performing experiments. Since no abnormalities were observed in this study, no animals or samples were excluded from analysis. Animals were randomly assigned groups for studies. Data were assessed for normal distribution and similar variance between groups before further analysis. Significance was assessed by independent two–tailed Student's t–tests, analysis of variance (ANOVA). Bonferroni correction was used when multiple comparisons were performed. P values less than 0.05 were considered significant. Data were expressed as mean ± SD.

Supplementary Material

Refer to Web version on PubMed Central for supplementary material.

ACKNOWLEDGEMENTS

This work was supported by grants from National Institute of Dental and Craniofacial Research, National Institutes of Health, Department of Health and Human Services (R01DE017449 and R01DE019932 to S.S.), grants from the National Natural Science Foundation of China (No. 81020108019 to Y. J. and S.S.) and the National Basic Research Program (973 Program) of China (No. 2011CB964700 to Y. J.).

REFERENCES

Akiyama K, Chen C, Wang D, Xu X, Qu C, Yamaza T, Cai T, Chen W, Sun L, Shi S. Mesenchymal-stem-cell-induced immunoregulation involves FAS-ligand-/FAS-mediated T cell apoptosis. Cell Stem Cell. 2012; 10:544–555. [PubMed: 22542159]

Augello A, Tasso R, Negrini SM, Cancedda R, Pennesi G. Cell therapy using allogeneic bone marrow mesenchymal stem cells prevents tissue damage in collagen-induced arthritis. Arthritis Rheum. 2007; 56:1175–1186. [PubMed: 17393437]

Azmi AS, Bao B, Sarkar FH. Exosomes in cancer development, metastasis, and drug resistance: a comprehensive review. Cancer Metastasis Rev. 2013; 32:623–642. [PubMed: 23709120]

Bechtel W, McGoohan S, Zeisberg EM, Muller GA, Kalbacher H, Salant DJ, Muller CA, Kalluri R, Zeisberg M. Methylation determines fibroblast activation and fibrogenesis in the kidney. Nat Med. 2010; 16:544–550. [PubMed: 20418885]

Bernardo ME, Fibbe WE. Mesenchymal stromal cells: sensors and switchers of inflammation. Cell Stem Cell. 2013; 13:392–402. [PubMed: 24094322]

Challen GA, Sun D, Jeong M, Luo M, Jelinek J, Berg JS, Bock C, Vasanthakumar A, Gu H, Xi Y, et al. Dnmt3a is essential for hematopoietic stem cell differentiation. Nat Genet. 2012; 44:23–31. [PubMed: 22138693]

Choi H, Lee RH, Bazhanov N, Oh JY, Prockop DJ. Anti-inflammatory protein TSG-6 secreted by activated MSCs attenuates zymosan-induced mouse peritonitis by decreasing TLR2/NF-kappaB signaling in resident macrophages. Blood. 2011; 118:330–338. [PubMed: 21551236]

Clark EA, Kalomoiris S, Nolta JA, Fierro FA. Concise review: MicroRNA function in multipotent mesenchymal stromal cells. Stem Cells. 2014; 32:1074–1082. [PubMed: 24860868]

Copelan EA. Hematopoietic stem-cell transplantation. N Engl J Med. 2006; 354:1813–1826. [PubMed: 16641398]

Denis H, Ndlovu MN, Fuks F. Regulation of mammalian DNA methyltransferases: a route to new mechanisms. EMBO Rep. 2011; 12:647–656. [PubMed: 21660058]

Dong Y, Jesse AM, Kohn A, Gunnell LM, Honjo T, Zuscik MJ, O'Keefe RJ, Hilton MJ. RBPjkappa-dependent Notch signaling regulates mesenchymal progenitor cell proliferation and differentiation during skeletal development. Development. 2010; 137:1461–1471. [PubMed: 20335360]

Garzon R, Liu S, Fabbri M, Liu Z, Heaphy CE, Callegari E, Schwind S, Pang J, Yu J, Muthusamy N, et al. MicroRNA-29b induces global DNA hypomethylation and tumor suppressor gene reexpression in acute myeloid leukemia by targeting directly DNMT3A and 3B and indirectly DNMT1. Blood. 2009; 113:6411–6418. [PubMed: 19211935]

Golden SA, Christoffel DJ, Heshmati M, Hodes GE, Magida J, Davis K, Cahill ME, Dias C, Ribeiro E, Ables JL, et al. Epigenetic regulation of RAC1 induces synaptic remodeling in stress disorders and depression. Nat Med. 2013; 19:337–344. [PubMed: 23416703]

Gonzalez MA, Gonzalez-Rey E, Rico L, Buscher D, Delgado M. Adipose-derived mesenchymal stem cells alleviate experimental colitis by inhibiting inflammatory and autoimmune responses. Gastroenterology. 2009; 136:978–989. [PubMed: 19135996]

Hatzistergos KE, Quevedo H, Oskouei BN, Hu Q, Feigenbaum GS, Margitich IS, Mazhari R, Boyle AJ, Zambrano JP, Rodriguez JE, et al. Bone marrow mesenchymal stem cells stimulate cardiac stem cell proliferation and differentiation. Circ Res. 2010; 107:913–922. [PubMed: 20671238]

Hilton MJ, Tu X, Wu X, Bai S, Zhao H, Kobayashi T, Kronenberg HM, Teitelbaum SL, Ross FP, Kopan R, et al. Notch signaling maintains bone marrow mesenchymal progenitors by suppressing osteoblast differentiation. Nat Med. 2008; 14:306–314. [PubMed: 18297083]

Islam MN, Das SR, Emin MT, Wei M, Sun L, Westphalen K, Rowlands DJ, Quadri SK, Bhattacharya S, Bhattacharya J. Mitochondrial transfer from bone-marrow-derived stromal cells to pulmonary alveoli protects against acute lung injury. Nat Med. 2012; 18:759–765. [PubMed: 22504485]

Kapinas K, Kessler C, Ricks T, Gronowicz G, Delany AM. miR-29 modulates Wnt signaling in human osteoblasts through a positive feedback loop. J Biol Chem. 2010; 285:25221–25231. [PubMed: 20551325]

Kelly TK, De Carvalho DD, Jones PA. Epigenetic modifications as therapeutic targets. Nat Biotechnol. 2010; 28:1069–1078. [PubMed: 20944599]

Le Blanc K, Frassoni F, Ball L, Locatelli F, Roelofs H, Lewis I, Lanino E, Sundberg B, Bernardo ME, Remberger M, et al. Mesenchymal stem cells for treatment of steroid-resistant, severe, acute graft-versus-host disease: a phase II study. Lancet. 2008; 371:1579–1586. [PubMed: 18468541]

Le Blanc K, Rasmusson I, Sundberg B, Gotherstrom C, Hassan M, Uzunel M, Ringden O. Treatment of severe acute graft-versus-host disease with third party haploidentical mesenchymal stem cells. Lancet. 2004; 363:1439–1441. [PubMed: 15121408]

Li CJ, Cheng P, Liang MK, Chen YS, Lu Q, Wang JY, Xia ZY, Zhou HD, Cao X, Xie H, et al. MicroRNA-188 regulates age-related switch between osteoblast and adipocyte differentiation. J Clin Invest. 2015; 125:1509–1522. [PubMed: 25751060]

Li W, Ren G, Huang Y, Su J, Han Y, Li J, Chen X, Cao K, Chen Q, Shou P, et al. Mesenchymal stem cells: a double-edged sword in regulating immune responses. Cell Death Differ. 2012; 19:1505–1513. [PubMed: 22421969]

Li Z, Hassan MQ, Jafferji M, Aqeilan RI, Garzon R, Croce CM, van Wijnen AJ, Stein JL, Stein GS, Lian JB. Biological functions of miR-29b contribute to positive regulation of osteoblast differentiation. J Biol Chem. 2009; 284:15676–15684. [PubMed: 19342382]

Li Z, Rana TM. Therapeutic targeting of microRNAs: current status and future challenges. Nat Rev Drug Discov. 2014; 13:622–638. [PubMed: 25011539]

Liang J, Zhang H, Hua B, Wang H, Wang J, Han Z, Sun L. Allogeneic mesenchymal stem cells transplantation in treatment of multiple sclerosis. Mult Scler. 2009; 15:644–646. [PubMed: 19389752]

Liu Y, Wang L, Kikuiri T, Akiyama K, Chen C, Xu X, Yang R, Chen W, Wang S, Shi S. Mesenchymal stem cell-based tissue regeneration is governed by recipient T lymphocytes via IFN-gamma and TNF-alpha. Nat Med. 2011; 17:1594–1601. [PubMed: 22101767]

Luga V, Zhang L, Viloria-Petit AM, Ogunjimi AA, Inanlou MR, Chiu E, Buchanan M, Hosein AN, Basik M, Wrana JL. Exosomes mediate stromal mobilization of autocrine Wnt-PCP signaling in breast cancer cell migration. Cell. 2012; 151:1542–1556. [PubMed: 23260141]

Mittelbrunn M, Sanchez-Madrid F. Intercellular communication: diverse structures for exchange of genetic information. Nat Rev Mol Cell Biol. 2012; 13:328–335. [PubMed: 22510790]

Nemeth K, Leelahavanichkul A, Yuen PS, Mayer B, Parmelee A, Doi K, Robey PG, Leelahavanichkul K, Koller BH, Brown JM, et al. Bone marrow stromal cells attenuate sepsis via prostaglandin E(2)-dependent reprogramming of host macrophages to increase their interleukin-10 production. Nat Med. 2009; 15:42–49. [PubMed: 19098906]

Ostrowski M, Carmo NB, Krumeich S, Fanget I, Raposo G, Savina A, Moita CF, Schauer K, Hume AN, Freitas RP, et al. Rab27a and Rab27b control different steps of the exosome secretion pathway. Nat Cell Biol. 2010; 12:19–30. sup pp 11-13. [PubMed: 19966785]

Pan W, Zhu S, Yuan M, Cui H, Wang L, Luo X, Li J, Zhou H, Tang Y, Shen N. MicroRNA-21 and microRNA-148a contribute to DNA hypomethylation in lupus CD4+ T cells by directly and indirectly targeting DNA methyltransferase 1. J Immunol. 2010; 184:6773–6781. [PubMed: 20483747]

Peinado H, Aleckovic M, Lavotshkin S, Matei I, Costa-Silva B, Moreno-Bueno G, Hergueta-Redondo M, Williams C, Garcia-Santos G, Ghajar C, et al. Melanoma exosomes educate bone marrow progenitor cells toward a pro-metastatic phenotype through MET. Nat Med. 2012; 18:883–891. [PubMed: 22635005]

Peng L, Xie DY, Lin BL, Liu J, Zhu HP, Xie C, Zheng YB, Gao ZL. Autologous bone marrow mesenchymal stem cell transplantation in liver failure patients caused by hepatitis B: short-term and long-term outcomes. Hepatology. 2011; 54:820–828. [PubMed: 21608000]

Portela A, Esteller M. Epigenetic modifications and human disease. Nat Biotechnol. 2010; 28:1057–1068. [PubMed: 20944598]

Qin H, Zhu X, Liang J, Wu J, Yang Y, Wang S, Shi W, Xu J. MicroRNA-29b contributes to DNA hypomethylation of CD4+ T cells in systemic lupus erythematosus by indirectly targeting DNA methyltransferase 1. J Dermatol Sci. 2013; 69:61–67. [PubMed: 23142053]

Rahman A, Isenberg DA. Systemic lupus erythematosus. N Engl J Med. 2008; 358:929–939. [PubMed: 18305268]

Ren G, Chen X, Dong F, Li W, Ren X, Zhang Y, Shi Y. Concise review: mesenchymal stem cells and translational medicine: emerging issues. Stem Cells Transl Med. 2012; 1:51–58. [PubMed: 23197640]

Sakaida I, Terai S, Yamamoto N, Aoyama K, Ishikawa T, Nishina H, Okita K. Transplantation of bone marrow cells reduces CCl4-induced liver fibrosis in mice. Hepatology. 2004; 40:1304–1311. [PubMed: 15565662]

Soifer HS, Rossi JJ, Saetrom P. MicroRNAs in disease and potential therapeutic applications. Mol Ther. 2007; 15:2070–2079. [PubMed: 17878899]

Sun L, Akiyama K, Zhang H, Yamaza T, Hou Y, Zhao S, Xu T, Le A, Shi S. Mesenchymal stem cell transplantation reverses multiorgan dysfunction in systemic lupus erythematosus mice and humans. Stem Cells. 2009; 27:1421–1432. [PubMed: 19489103]

Teachey DT, Seif AE, Brown VI, Bruno M, Bunte RM, Chang YJ, Choi JK, Fish JD, Hall J, Reid GS, et al. Targeting Notch signaling in autoimmune and lymphoproliferative disease. Blood. 2008; 111:705–714. [PubMed: 17925488]

Thery C, Amigorena S, Raposo G, Clayton A. Isolation and characterization of exosomes from cell culture supernatants and biological fluids. Curr Protoc Cell Biol. 2006 *Chapter 3*, Unit 3 22.

Thery C, Zitvogel L, Amigorena S. Exosomes: composition, biogenesis and function. Nat Rev Immunol. 2002; 2:569–579. [PubMed: 12154376]

Tsai CC, Su PF, Huang YF, Yew TL, Hung SC. Oct4 and Nanog directly regulate Dnmt1 to maintain self-renewal and undifferentiated state in mesenchymal stem cells. Mol Cell. 2012a; 47:169–182. [PubMed: 22795133]

Tsai HC, Li H, Van Neste L, Cai Y, Robert C, Rassool FV, Shin JJ, Harbom KM, Beaty R, Pappou E, et al. Transient low doses of DNA-demethylating agents exert durable antitumor effects on hematological and epithelial tumor cells. Cancer Cell. 2012b; 21:430–446. [PubMed: 22439938]

Uccelli A, Moretta L, Pistoia V. Mesenchymal stem cells in health and disease. Nat Rev Immunol. 2008; 8:726–736. [PubMed: 19172693]

Wang D, Zhang H, Liang J, Li X, Feng X, Wang H, Hua B, Liu B, Lu L, Gilkeson GS, et al. Allogeneic mesenchymal stem cell transplantation in severe and refractory systemic lupus erythematosus: 4 years experience. Cell Transplant. 2012

Zhang Z, Cai YQ, Zou F, Bie B, Pan ZZ. Epigenetic suppression of GAD65 expression mediates persistent pain. Nat Med. 2011; 17:1448–1455. [PubMed: 21983856]

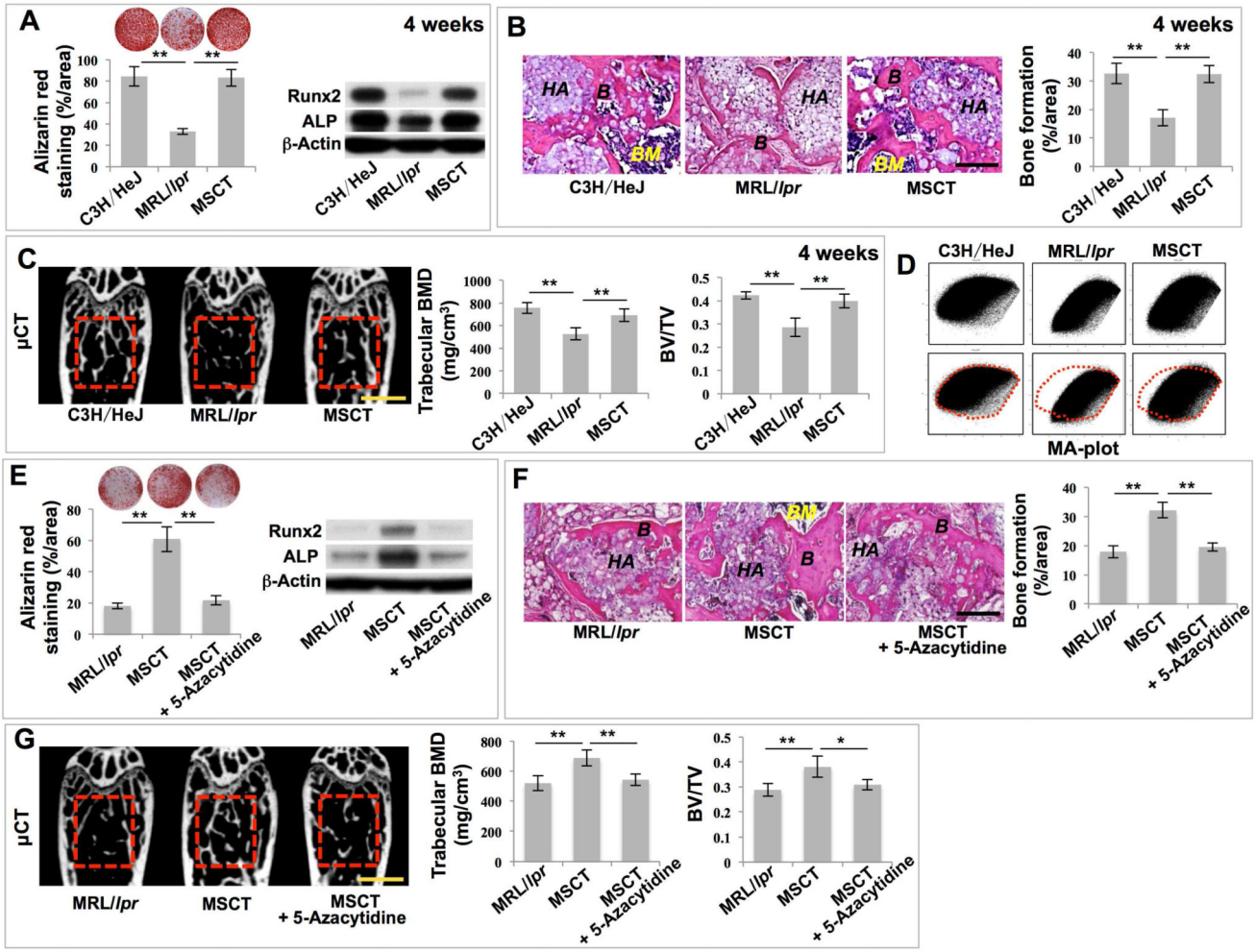

Figure 1. MSC transplantation (MSCT) rescued impaired BMMSC functions and osteoporotic phenotype in MRL/*lpr* mice *via* regulation of DNA methylation profile

(**A**) Alizarin red staining showed mineralized nodule formation of BMMSCs derived from wild-type C3H/HeJ mice (C3H/HeJ), MRL/*lpr* mice (MRL/*lpr*) and MRL/*lpr* mice at 4 weeks post-MSCT. n = 5. Western blot showed expression of Runx2 and ALP in BMMSCs. β-Actin was used as a loading control. (**B**) H&E staining showed formation of new bone (*B*) and bone marrow (*BM*) around HA/TCP (*HA*) carrier when BMMSCs were implanted into immunocompromised mice. n = 5. (**C**) μCT analysis of bone mineral density (BMD) and bone volume/total volume (BV/TV) of femurs. n = 5. (**D**) MA plot showed global methylation patterns of gene promoters in BMMSCs, as assessed by DNA methylation microarray. (**E**) Alizarin red staining showed mineralized nodule formation by BMMSCs. n = 5. Western blot showed expressions of Runx2 and ALP in BMMSCs. (**F**) H&E staining showed formation of new bone (*B*) and bone marrow (*BM*) around HA/TCP (*HA*) carrier when BMMSCs were implanted into immunocompromised mice. n = 5. (**G**) μCT analysis of BMD and BV/TV of femurs. n = 5. All results are representative of data generated in three independent experiments except DNA methylation microarray analysis. Statistical

significance was determined with one-way analysis of variance (ANOVA). **$P < 0.01$; *$P < 0.05$. Error bars: mean ± SD; 200 μm (**B, F**), 1 mm (**C, G**).

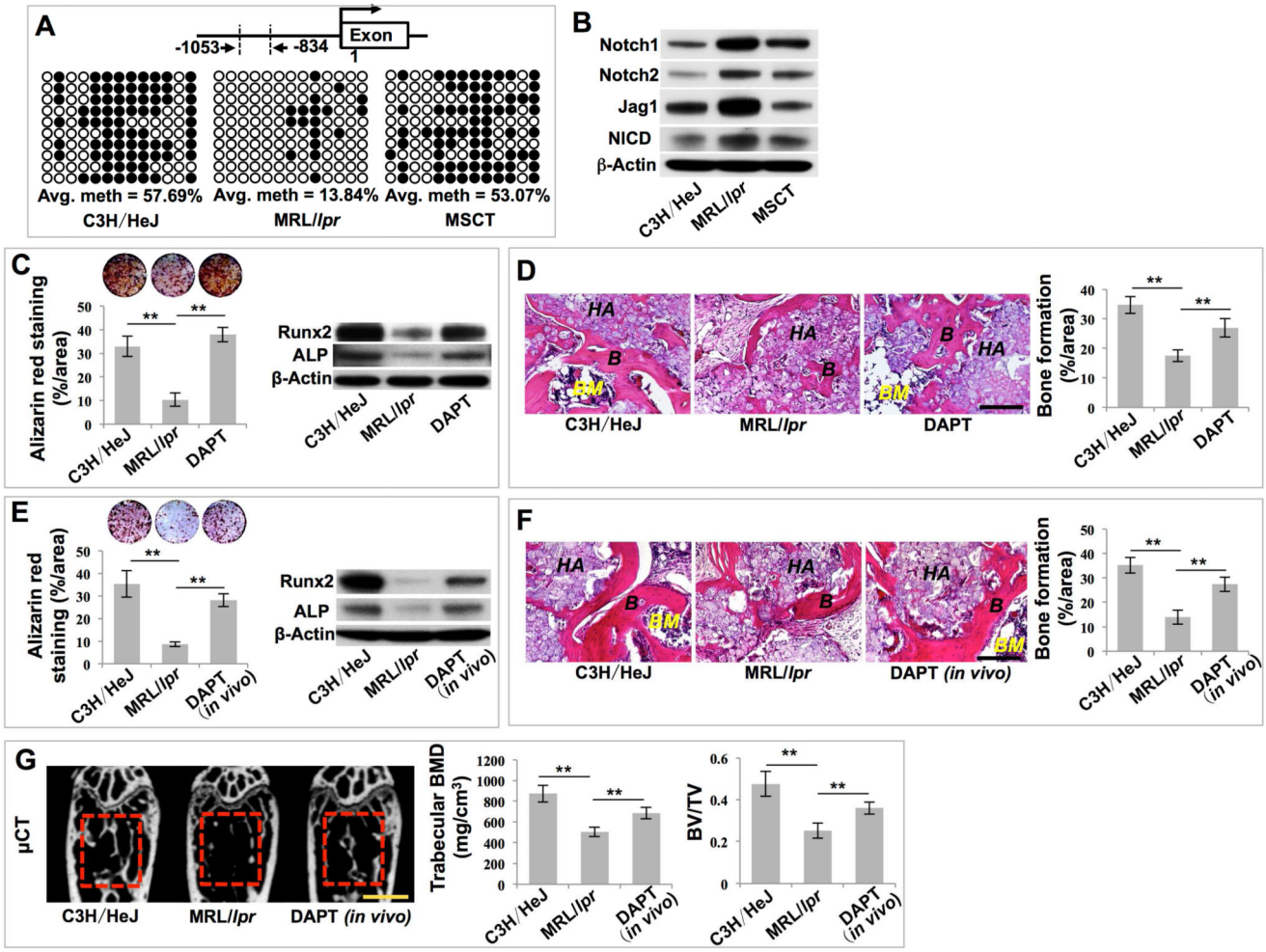

Figure 2. MSCT inhibited Notch signaling in recipient MRL/*lpr* BMMSCs *via* regulating DNA methylation in Notch1 promoter region

(**A**) Bisulfite genomic sequencing analysis of BMMSC Notch1 promoter region. Each box is representative of the indicated BMMSC sample; each row of dots is representative of the CpG island in the *Notch1* promoter region; each dot is representative of a single CpG. Empty dots indicate unmethylated CpGs; black dots indicate methylated CpGs. Each row represents a single sequenced clone (ten for each sample). (**B**) Western blot showed Notch1, Notch2, Jag1 and NICD expression in BMMSCs. (**C**) Alizarin red staining showed mineralized nodule formation by BMMSCs. n = 5. Western blot showed expressions of Runx2 and ALP in BMMSCs. (**D**) H&E staining showed formation of new bone (*B*) and bone marrow (*BM*) around HA/TCP (*HA*) carrier when BMMSCs were implanted into immunocompromised mice. n = 5. (**E**) Alizarin red staining showed mineralized nodule formation by BMMSCs. n = 5. Western blot showed expression of Runx2 and ALP in BMMSCs. (**F**) H&E staining showed formation of new bone (*B*) and bone marrow (*BM*) around HA/TCP (*HA*) carrier when BMMSCs were implanted into immunocompromised mice. n = 5. (**G**) μCT analysis of BMD and BV/TV of femurs. n = 5. All results are representative of data generated in three independent experiments. Statistical significance

was determined with one-way ANOVA. **$P < 0.01$. Error bars: mean ± SD, 200 μm (**D, F**), 1 mm (**G**).

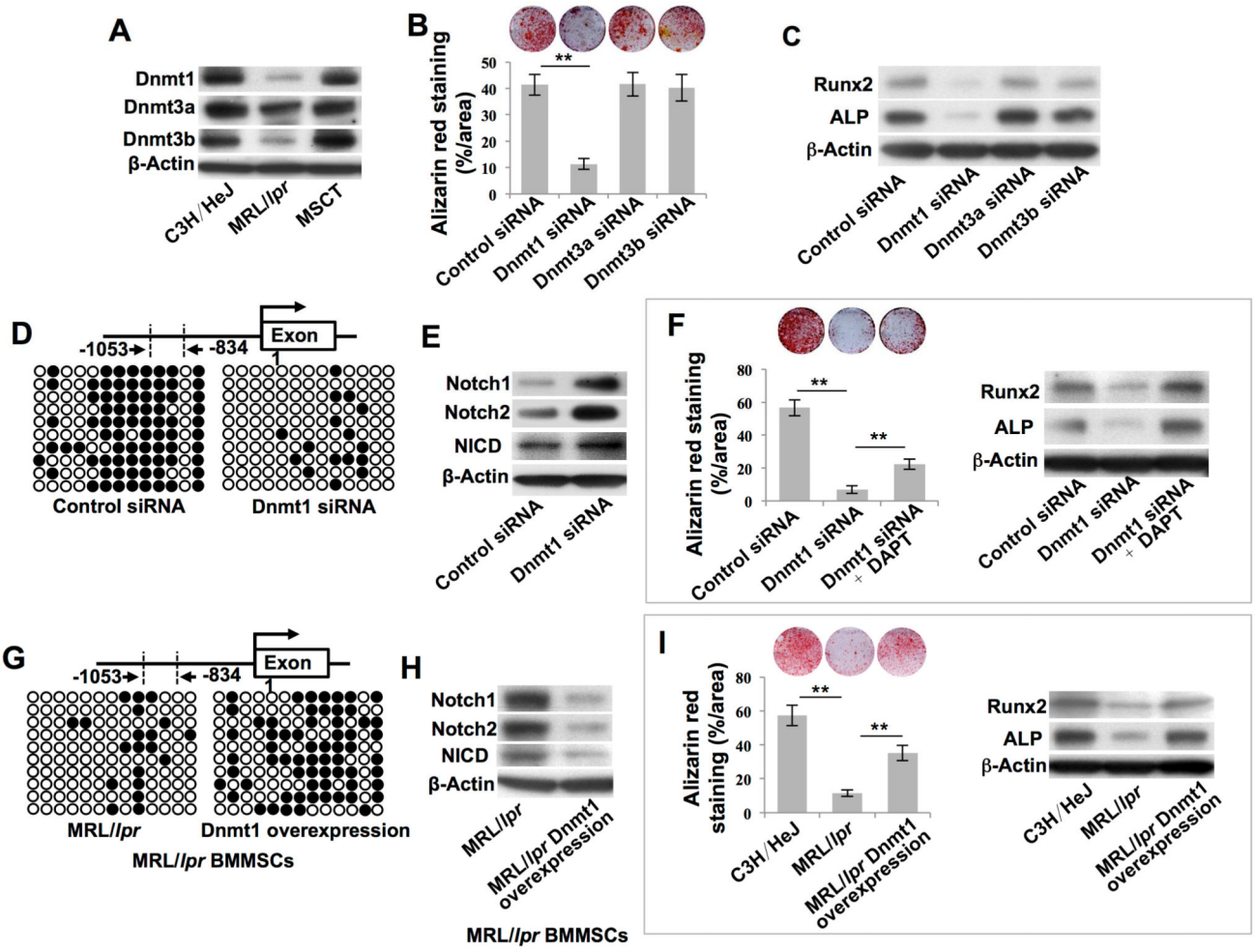

Figure 3. MSCT rescued hypomethylation of the *Notch* gene promoter in recipient MRL/*lpr* BMMSCs *via* upregulation of Dnmt1

(**A**) Western blot showed Dnmt1, Dnmt3a and Dnmt3b expression in BMMSCs. (**B**) Alizarin red staining showed mineralized nodule formation by BMMSCs. n = 4. (**C**) Western blot showed Runx2 and ALP expression in BMMSCs. (**D, G**) Bisulfite genomic sequencing analysis of BMMSC Notch1 promoter region. (**E, H**) Western blot showed Notch1, Notch2 and NICD expression in BMMSCs. (**F, I**) Alizarin red staining showed mineralized nodule formation by BMMSCs. n = 4. Western blot showed Runx2 and ALP expression in BMMSCs. All results are representative of data generated in three independent experiments. Statistical significance was determined with one-way ANOVA. $^{**}P < 0.01$. Error bars: mean ± SD.

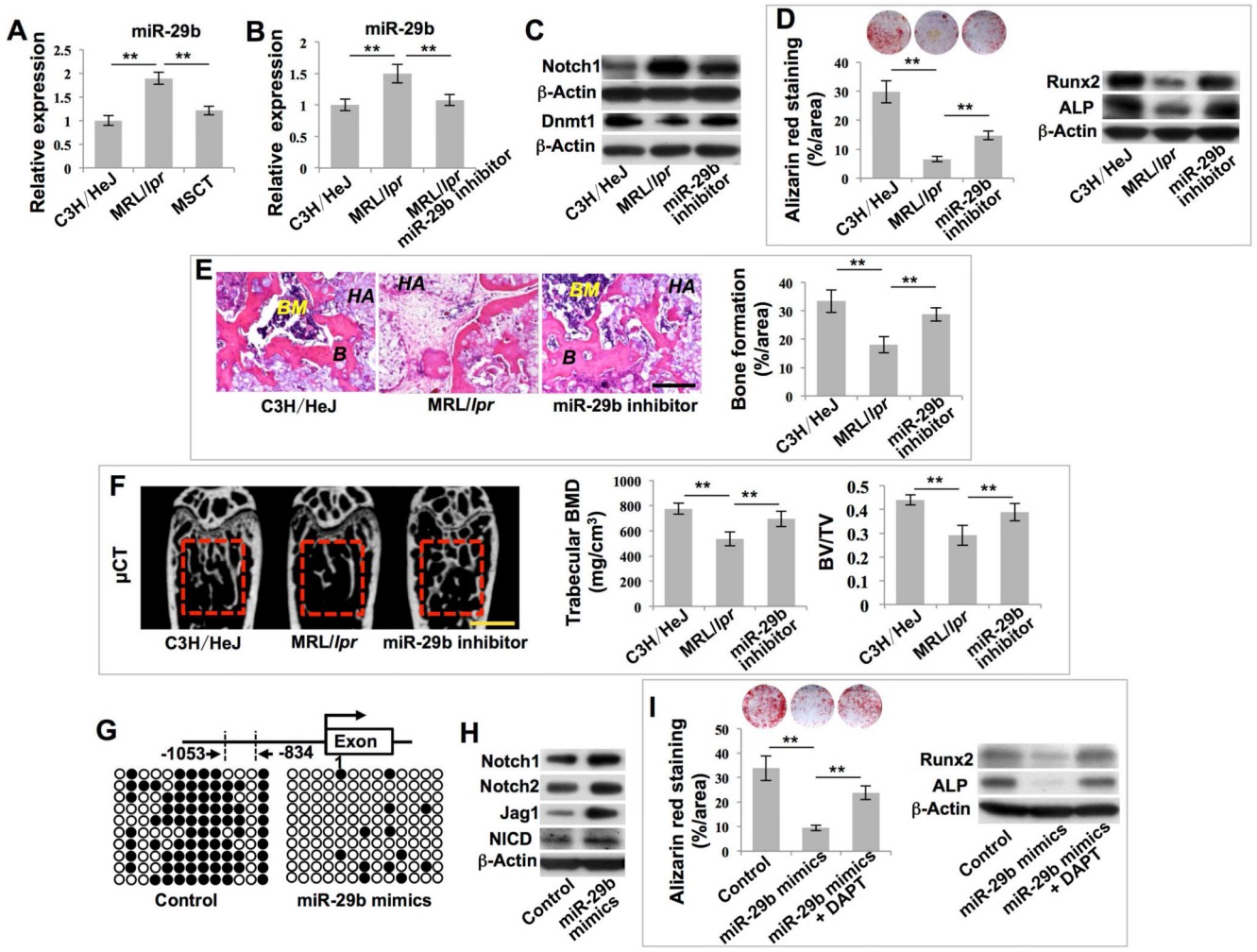

Figure 4. MSCT governed Dnmt1-mediated DNA methylation of the *Notch1* promoter *via* regulating intracellular levels of miR-29b

(**A, B**) Real-time PCR showed miR-29b expression in BMMSCs. n = 5. (**C**) Western blot showed Notch1 and Dnmt1 expression in BMMSCs. (**D**) Alizarin red staining showed mineralized nodule formation by BMMSCs. n = 5. Western blot showed Runx2 and ALP expression in BMMSCs. (**E**) H&E staining showed formation of new bone (*B*) and bone marrow (*BM*) around HA/TCP (*HA*) carrier when BMMSCs were implanted into immunocompromised mice. n = 5. (**F**) μCT analysis showed BMD and BV/TV of femurs. n = 5. (**G**) Bisulfite genomic sequencing analysis of BMMSC Notch1 promoter region. (**H**) Western blot showed Notch1, Notch2, Jag1 and NICD expression in BMMSCs. (**I**) Alizarin red staining showed mineralized nodule formation by BMMSCs. n = 4. Western blot showed Runx2 and ALP expression in BMMSCs. All results are representative of data generated in three independent experiments. Statistical significance was determined with one-way ANOVA. $^{**}P < 0.01$. Error bars: mean ± SD, 200 μm (**E**), 1 mm (**F**).

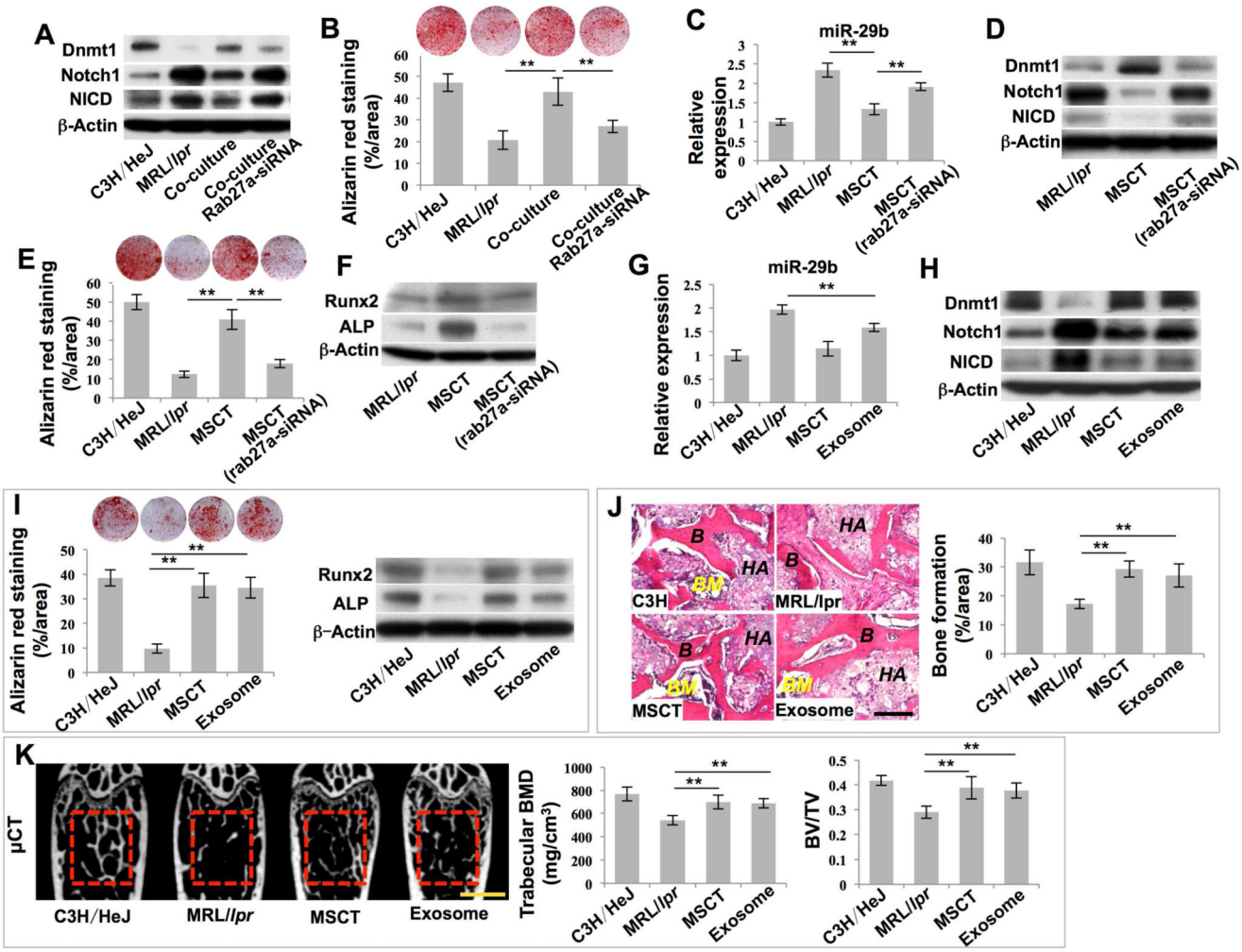

Figure 5. Exosomes secreted due to MSCT downregulated intracellular levels of miR-29b in recipient MRL/*lpr* BMMSCs

(**A**) Western blot showed Dnmt1, Notch1 and NICD expression in BMMSCs. (**B**) Alizarin red staining showed mineralized nodule formation by BMMSCs. n = 4. (**C**) Real-time PCR showed miR-29b expression in BMMSCs. n = 5. (**D**) Western blot showed Dnmt1, Notch1 and NICD expression in BMMSCs. (**E**) Alizarin red staining showed mineralized nodule formation of BMMSCs. n = 5. (**F**) Western blot showed Runx2 and ALP expression in BMMSCs. (**G**) Real-time PCR showed miR-29b expression in BMMSCs. n = 5. (**H**) Western blot showed Dnmt1, Notch1 and NICD expression in BMMSCs. (**I**) Alizarin red staining showed mineralized nodule formation by BMMSCs. n = 5. Western blot showed Runx2 and ALP expression in BMMSCs. (**J**) H&E staining showed formation of new bone (*B*) and bone marrow (*BM*) around HA/TCP (*HA*) carrier when BMMSCs were implanted into immunocompromised mice. n = 5. (**K**) μCT analysis of BMD and BV/TV of femurs. n = 5. All results are representative of data generated in three independent experiments. Statistical significance was determined with one-way ANOVA. $^{**}P < 0.01$. Error bars: mean ± SD, 200 μm (**J**), 1 mm (**K**).

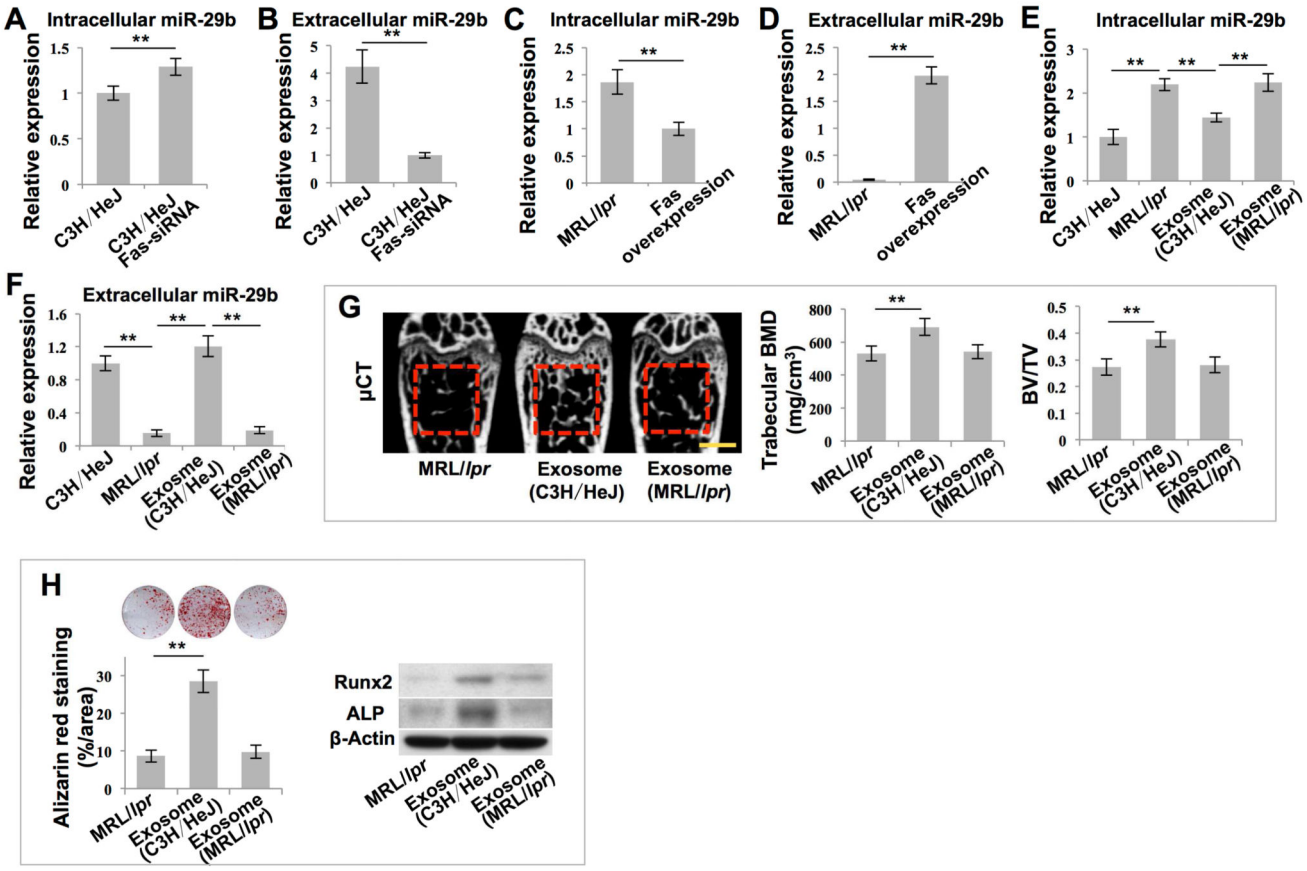

Figure 6. Exosomes rescued intracellular levels of miR-29b in MRL/*lpr* BMMSCs

(**A-F**) Real-time PCR showed miR-29b expression in BMMSCs under indicated conditions. n = 6. (**G**) μCT analysis of BMD and BV/TV of femurs. n = 5. (**H**) Alizarin red staining showed mineralized nodule formation by BMMSCs. n = 5. Western blot showed Runx2 and ALP expression in BMMSCs. All results are representative of data generated in three independent experiments. Statistical significance was determined with two–tailed Student's t–tests (**A-D**) or one-way ANOVA (**E-H**). ***P* < 0.01. Error bars: mean ± SD, 1 mm (**G**).

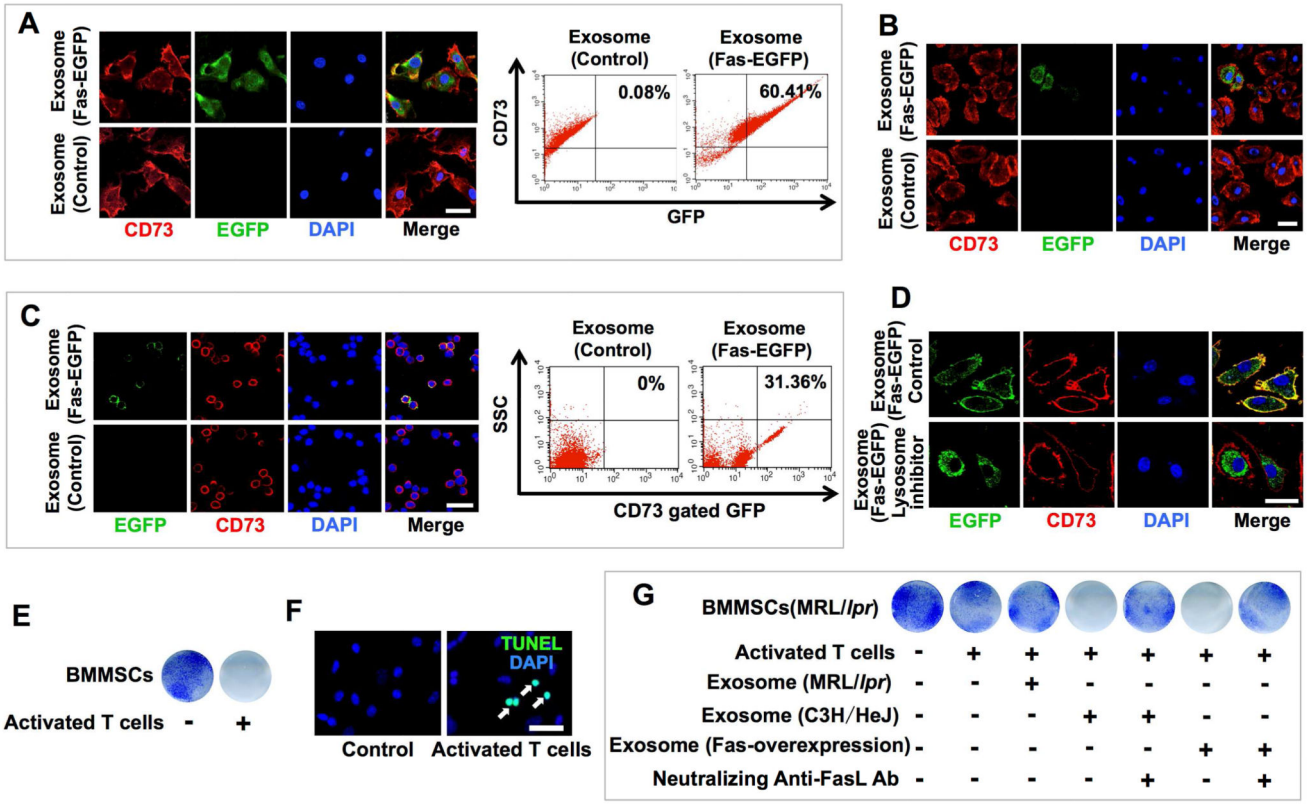

Figure 7. MRL/*lpr* BMMSCs reused Fas through donor MSC-released exosomes

(**A**) Detection of EGFP$^+$ and CD73$^+$ cells among cultured BMMSCs by immunofluorescence and flow cytometric analysis after *in vitro* Fas-EGFP$^+$ exosome treatment. CD73 was used as a BMMSC marker for co-staining. (**B**) Detection of EGFP$^+$ and CD73$^+$ cells among cultured BMMSCs by immunofluorescence after *in vivo* Fas-EGFP$^+$ exosome infusion. (**C**) Detection of EGFP$^+$ and CD73$^+$ cells among cultured BMMSCs by immunofluorescence and flow cytometric analysis after *in vivo* Fas-EGFP$^+$ exosome infusion. (**D**) After pretreatment with lysosome inhibitor and treatment with Fas-EGFP$^+$ exosomes, EGFP$^+$ and CD73$^+$ cells among the BMMSCs were detected by immunofluorescence. (**E**) The reduced number of toluidine blue positive cells indicated C3H/HeJ BMMSC apoptosis after direct co-culture with activated spleen T cells. (**F**) TUNEL staining (white arrows) of apoptotic BMMSCs. (**G**) Toluidine blue staining of MRL/*lpr* BMMSCs co-cultured with activated spleen T cells under indicated conditions. All results are representative of data generated in three independent experiments. Error bars: 25 μm (**A-C, F**), 20 μm (**D**).